BUTTERWORTH HEINEMANN

Three-dimensional particle-tracking velocimetry measurement of turbulence statistics and energy budget in a backward-facing step flow

Nobuhide Kasagi and Akio Matsunaga
Department of Mechanical Engineering, The University of Tokyo, Bunkyo-ku, Tokyo, Japan

Using a three-dimensional (3-D) particle-tracking velocimeter, detailed turbulent flow measurements were made in a plane channel with a one-sided 50% abrupt expansion, which acted as a backward-facing step. The turbulent channel flow reached a fully developed state well upstream of the step. The Reynolds number based on the upstream centerline velocity and the step height H was 5540. With the mean reattachment point located at $6.51H$ downstream of the step, the measurement region ranged from $-2H$ upstream to $12H$ downstream of the step. Various turbulent statistics and the energy budget were calculated from numerous instantaneous vector distributions. As in previous experimental investigations, the Reynolds normal and shear stresses had maximum values upstream of the reattachment. The stress anisotropy tensor revealed a peculiar phenomenon near the reattachment wall, wherein the spanwise normal stress was the largest among the three normal stresses. The triple velocity correlations indicated large values in the separating shear layer, and hence the turbulent diffusion was a major term in the energy budget. Comparison was made between the present results and those of the direct numerical simulation (DNS) of Le et al. (1993), and it was found that the mean and fluctuating velocities, the Reynolds shear stress, and the turbulent energy budget were in excellent agreement, although there was a considerable difference in the inflow conditions.

Keywords: turbulence; separated flow; backward-facing step; particle-tracking velocimeter; turbulent statistics; energy budget

Introduction

Flow separation and reattachment are of great importance in such fields as aeronautical, mechanical, civil, and chemical engineering, and in the environment, because their frequent occurrence may affect fundamental flow characteristics and result in a drastic change in the performance of fluid machinery and heat transfer devices. Hence, any modern computational fluid dynamics code should be tested in a flow problem with separation and reattachment. In particular, the accuracy of numerical schemes and turbulence models should be thoroughly evaluated. Among a number of flows with separation and reattachment, the flow over a backward-facing step is one of those with the simplest geometries; however, when it is turbulent, the flow structure is very complex, and much remains to be explored.

Up to the present, many investigators have attempted turbulence measurements in the backward-facing step flow using various measurement techniques (Eaton and Johnston 1981). However, the use of hot-wire and hot-film anemometers should be generally limited to flows without flow reversal and separation. Laser velocimeters offer the great advantage of being capable of measuring a reverse flow without disturbing the flow field, but their traverse is often associated with considerable difficulty. In addition, with the measurement techniques above, only two of the three velocity components have been simultaneously measured up to the present (e.g., Abbott and Kline 1962; Adams and Johnston 1988; Chandrsuda and Bradshaw 1981; Driver and Seegmiller 1985), although information on all Reynolds stress tensor components is indispensable for current turbulence modeling. Moreover, recent direct and large-eddy simulations of a backward-facing step flow (Akselvoll and Moin 1993; Le et al. 1993; Neto et al. 1993) preferably should be verified against not only measured turbulent stresses but also their budgets.

Recent developments in digital image processing have made it possible to measure an instantaneous vector distribution in three-dimensional (3-D) space. The present technique, called 3-D particle-tracking velocimetry (3-D PTV, hereafter), was developed by Nishino et al. (1989) and has already been applied to various turbulent flows (Kasagi and Nishino 1991; Kasagi and Sata 1992). In particular, the measurement result of a turbulent channel flow obtained by Nishino and Kasagi (1989) showed excellent agreement with direct numerical simulations and demonstrated the reliability of this technique. Ninomiya and Kasagi (1993) obtained the Reynolds stress budgets in a self-pre-

Address reprint requests to Prof. Nobuhide Kasagi, Dept. of Mechanical Engineering, The University of Tokyo, Hongo 7-3-1, Bunkyo-ku, Tokyo 113, Japan.

Received 6 September 1994; accepted 8 June 1995

Int. J. Heat and Fluid Flow 16: 477–485, 1995

655 Avenue of the Americas, New York, NY 10010

0142-727X/95/$10.00
SSDI 0142-727X(95)00041-N

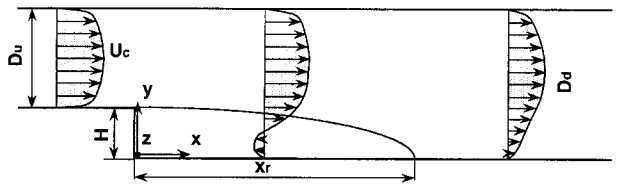

Figure 1 Flow field and coordinate system

serving turbulent axisymmetric jet in order to test the existing turbulence models. In the present work, 3-D PTV measurements were made of all three velocity components in turbulent separated and reattaching flow downstream of the one-sided expansion of a plane channel in order to obtain data of turbulent statistics at densely distributed measurement points and to calculate the turbulent kinetic energy budget. This particular flow geometry was selected mainly because the inflow condition is well defined as a fully developed channel flow so that no predictive calculation would suffer from incompleteness or ambiguity in the upstream boundary conditions.

Experimental setup and procedure

The flow field and coordinate system are shown in Figure 1. Experiments were performed in a closed-loop two-dimensional (2-D) water channel flow facility of the Mechanical Engineering Department of the University of Tokyo (for details, see Nishino and Kasagi 1989). The flow is driven by the static pressure difference between upper and lower reservoirs. The upstream developing section has a rectangular cross section of 81 mm in height D_u, and 800 mm in width and is about 6.6 m ($82.5D_u$) long. The height of the backward-facing step H is 41 mm, and the resultant expansion ratio is 1.504. Downstream of the step, the expanded channel has a length of 1.7 m and is connected with the lower reservoir. It was confirmed that flow reaches its fully developed state well upstream of the step. Three kinds of defined Reynolds numbers are calculated from the measured mean velocity distribution as $\mathrm{Re}_c = U_c D_u/\nu = 11010$, $\mathrm{Re}_b = U_b D_u/\nu = 9550$, and $\mathrm{Re}_\tau = u_\tau D_u/2\nu = 290$, where the centerline, bulk mean, and friction velocities are, respectively, $U_c = 129.7$ mm/s, $U_b = 112.5$ mm/s, and $u_\tau = 6.84$ mm/s, while $D_u = 81.3$ mm. These Reynolds number values are in good agreement with the empirical formula of Dean (1978), which is applicable to fully developed channel flows. The ratio of the step height to the channel width in the present experiment is 1 : 20, which should be large enough to assure a 2-D flow field. The water temperature was maintained at 20 ± 0.02°C throughout the experiment. The resultant Reynolds number based on the upstream centerline velocity and the step height $\mathrm{Re}_H = U_c H/\nu$ was 5,540.

Velocity vectors are measured by the 3-D PTV. Tracer particles are suspended in water and observed using three TV cameras fixed to the side of the test section. Successive TV frames acquired are sent to an image processor and then recorded by a laser disk recorder. The measurement volume is illuminated by a stroboscope, the flashes of which are triggered at 60 Hz at the beginning of alternate scans of the odd and even TV fields that constitute one TV frame. Consequently, two consecutive particle images are obtained at an interval of 1/60 s, and such an image pair is recorded at an interval of 1/10 s. Tracer particles used are Nylon 12, of which diameter and specific density were 210 ~ 250 μm and 1.02, respectively. These values ensure sufficient traceability of particles, although they are slightly heavier than water. The buoyancy effect only appeared in the spanwise velocity component, as described later.

The flow velocities are determined through the procedures described in detail by Kasagi and Nishino (1991); i.e., calculation of 3-D particle positions, particle tracking over 1/60 s, and vector tracking over 1/10 s. First, from a set of three instantaneous images taken by the TV cameras, a 3-D particle position is calculated as an intersection of corresponding perspective rays from the three cameras. Then, in particle tracking over 1/60 s, the particles are tracked over 1/60 s between odd and even TV fields. This is performed by defining a search volume around the initial position of a particle calculated from three odd TV fields and searching the volume for the particle's position calculated

Notation

B	bias limit
b_{ij}	anisotropy tensor, $b_{ij} = \overline{u_i u_j}/2k - \delta_{ij}/3$
D_u	channel width upstream of the step, Figure 1
D_d	channel width downstream of the step, Figure 1
H	step height
k	turbulent kinetic energy, $k = \overline{u_i u_i}/2$
Re_b	Reynolds number, $\mathrm{Re}_b = U_b D_u/\nu$
Re_c	Reynolds number, $\mathrm{Re}_c = U_c D_u/\nu$
Re_H	Reynolds number, $\mathrm{Re}_H = U_c H/\nu$
Re_τ	Reynolds number, $\mathrm{Re}_\tau = u_\tau D_u/2\nu$
S	precision index
t	Student t
U, V, W	mean velocity components in the x, y, and z directions
U_{95}	uncertainty interval at 95% coverage
u, v, w	fluctuating velocity components in the x, y, and z directions
u_i	fluctuating velocity component in the ith direction
$\overline{u_i u_j}$	Reynolds stress
$\overline{u_i u_j u_k}$	triple velocity correlations
u_τ	friction velocity, $u_\tau = (\tau_w/\rho)^{1/2}$
x, y, z	streamwise, wall-normal, and spanwise coordinates
x_i	ith coordinate
x_r	reattachment length

Greek

γ	forward flow fraction
ε	dissipation rate of k
ν	kinetic viscosity
ρ	density
τ	shear stress
Ψ	stream function

Subscripts

b	bulk mean value
c	value at upstream channel center
rms	root-mean-square value
u	value upstream of step
w	value at wall

Superscripts

$^+$	normalized by the wall variables, u_τ and ν
$^-$	ensemble average

Table 1 Precision index, bias limit, and uncertainty intervals at 95% coverage of measured velocity components *

	U_{95}, mm/s	B, mm/s	S, mm/s
u	0.485	0.112	0.236
v	0.564	0.125	0.276
w	0.636	0.133	0.311

* $U_{95} = [B^2 + (tS)^2]^{1/2}$

from three even TV fields. Presently, the search volume size is determined by referring to the velocity distributions preliminarily measured in the same experimental setup by Kawara and Kasagi (1989). Finally, vector tracking over 1/10 s is performed for two of 1/60 s vectors. Final correspondence between the vectors is established only when the one-to-one correspondence is attained by tracking in both forward and backward temporal directions. The velocity vector is then calculated based on the particle's displacement over 1/10 s. The above sequence of data processing is carried out automatically by the computer programs developed. The average data processing time was 40 s per frame.

The measurement was repeated for 17 volumes, which, as a whole, cover the flow field ranging from $-2H$ upstream to $12H$ downstream of the separation point. Each measurement volume was $80 \times 80 \times 80$ mm^3. The measurement time span was 4.5 ~ 7 min for each region, and this resulted in 1.9×10^5 images and 1.5×10^7 velocity vectors in total. All data of the turbulence statistics described below are calculated as an ensemble average

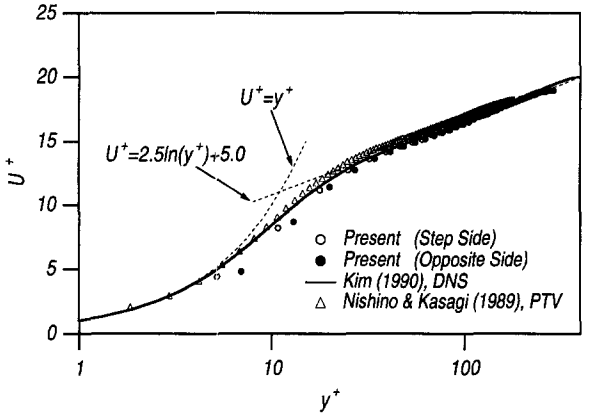

Figure 2 Streamwise mean velocity distribution upstream of the step

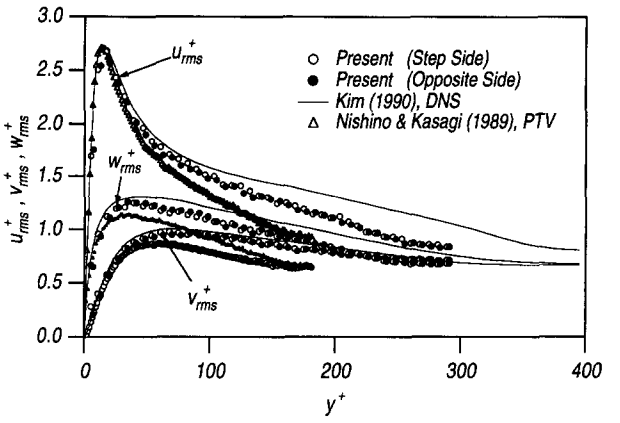

Figure 3 Distributions of root-mean-square turbulent velocity fluctuations upstream of the step

of 30 ~ 1000 vectors obtained in an averaging volume of about $\Delta x \times \Delta y = 2 \times 1$ (mm^2) under the assumption of spanwise homogeneity. Thus, the statistical data are distributed over 50×81 and 250×122 points upstream and downstream of the step, respectively. It is noted that the variation of the mean velocities in the averaging volume is linearly interpolated when the velocity fluctuations are calculated. The turbulence statistics thus obtained as ensemble averages are assigned to the gravitational center of the datapoints in the volume. Thus, the distribution of turbulence statistics is also considered linearly interpolated.

On the basis of ANSI/ASME PTC 19.1-1985, the measurement uncertainties associated with the present measurement are

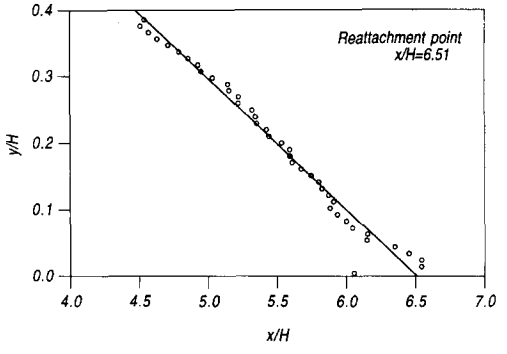

Figure 4 Location of 50% forward flow fraction

Table 2 Measured values and uncertainty intervals

Position	$x/H = 1.0$, $y/H = 1.94$	$x/H = 6.0$, $y/H = 0.99$
Number of vectors	845	413
U/U_c	$1.00 \pm 3.19 \times 10^{-3}$	$5.69 \times 10^{-1} \pm 1.56 \times 10^{-2}$
V/U_c	$-5.42 \times 10^{-3} \pm 2.71 \times 10^{-3}$	$-5.92 \times 10^{-2} \pm 1.08 \times 10^{-2}$
u_{rms}/U_c	$4.46 \times 10^{-2} \pm 3.57 \times 10^{-3}$	$1.59 \times 10^{-1} \pm 1.57 \times 10^{-2}$
v_{rms}/U_c	$3.68 \times 10^{-2} \pm 3.31 \times 10^{-3}$	$1.09 \times 10^{-1} \pm 1.09 \times 10^{-2}$
w_{rms}/U_c	$3.52 \times 10^{-2} \pm 3.41 \times 10^{-3}$	$1.19 \times 10^{-1} \pm 1.20 \times 10^{-2}$
$-\overline{uv}/U_c^2$	$1.77 \times 10^{-5} \pm 1.60 \times 10^{-4}$	$9.28 \times 10^{-3} \pm 2.41 \times 10^{-3}$
$\overline{u^3}/U_c^3$	$-4.99 \times 10^{-5} \pm 3.34 \times 10^{-5}$	$-2.10 \times 10^{-3} \pm 2.15 \times 10^{-3}$
$\overline{u^2v}/U_c^3$	$2.86 \times 10^{-6} \pm 8.73 \times 10^{-6}$	$1.02 \times 10^{-3} \pm 6.86 \times 10^{-4}$
$\overline{uv^2}/U_c^3$	$-2.12 \times 10^{-6} \pm 7.21 \times 10^{-6}$	$-8.55 \times 10^{-4} \pm 4.72 \times 10^{-4}$
$\overline{uw^2}/U_c^3$	$-8.80 \times 10^{-5} \pm 6.60 \times 10^{-6}$	$-7.96 \times 10^{-4} \pm 4.04 \times 10^{-4}$
$\overline{v^3}/U_c^3$	$6.29 \times 10^{-6} \pm 1.88 \times 10^{-5}$	$8.70 \times 10^{-4} \pm 7.00 \times 10^{-4}$
$\overline{vw^2}/U_c^3$	$3.52 \times 10^{-6} \pm 5.46 \times 10^{-6}$	$4.61 \times 10^{-4} \pm 2.66 \times 10^{-4}$

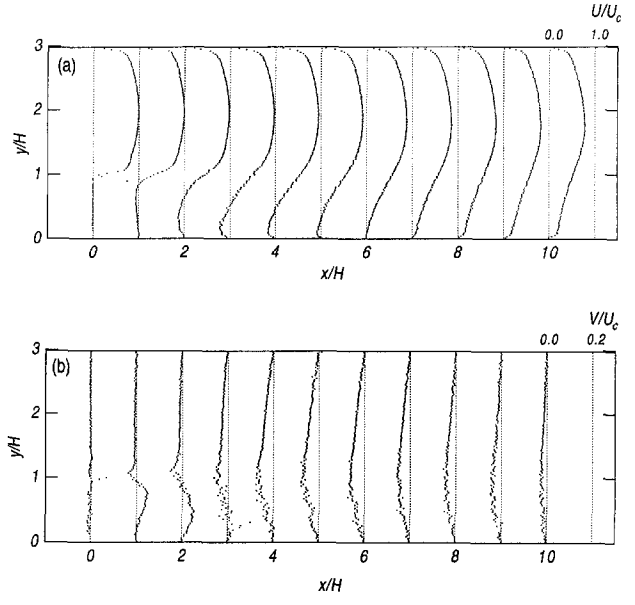

Figure 5 Mean velocity distributions: (a) streamwise component U/U_c, (b) wall-normal component V/U_c

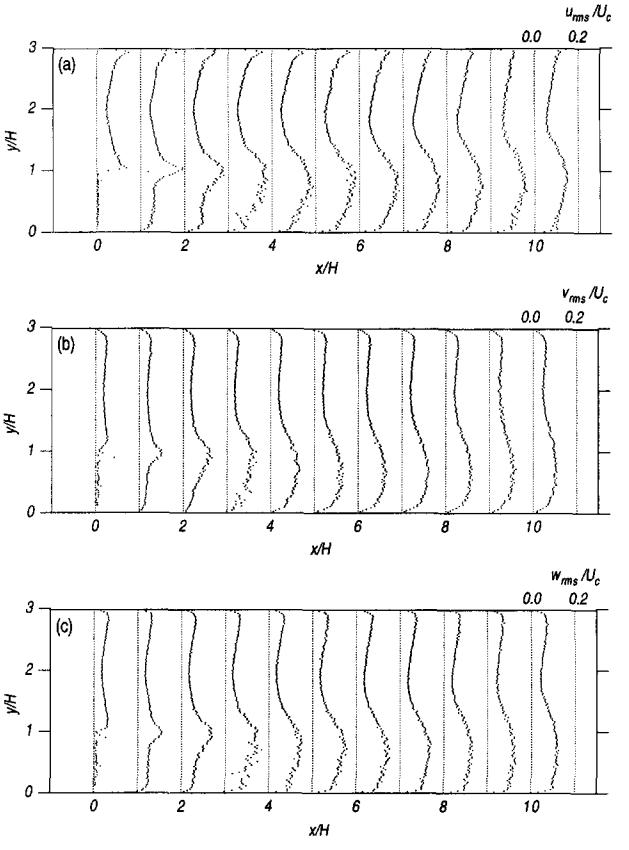

Figure 7 Root-mean-square turbulent velocity fluctuations: (a) streamwise component, (b) wall-normal component, (c) spanwise component

estimated by referring to Nishino et al. (1989). The precision index, the bias limit, and the resultant uncertainty intervals at 95% coverage of the measured instantaneous velocity components are summarized in Table 1. The uncertainty intervals associated with statistical quantities at typical positions are listed in Table 2. It is seen that those associated with higher-order moments are larger. The uncertainty interval is dependent upon the sample size, and hence it changes from position to position, but the degree of scatter of datapoints is a good indicator of the uncertainty interval at the remainder of the positions.

Experimental results and discussion

Flow upstream of separation

The distributions of streamwise mean velocity and root-mean-square turbulent velocity fluctuations upstream of the step are shown in Figures 2 and 3, respectively. The present data obtained over the entire cross section are divided into two sets denoted as those on the step side and the opposite side. They are compared with the results of direct numerical simulation (DNS, hereafter) of Kim (J. Kim, 1990, private communication) and the PTV measurement of Nishino and Kasagi (1989) in these figures. Note that these previous DNS and PTV results of fully developed channel flow are obtained at $Re_\tau = 395$ and 205, respectively, while the present one is obtained at $Re_\tau = 290$. Each quantity in the figures is nondimensionalized by the friction velocity, which is estimated by fitting an eddy–viscosity-based profile to the mean velocity data close to the wall (McEligot 1984). The two curves of mean velocity in the present study show a slight difference near the wall, but generally they are in good agreement with the DNS result. The data of Nishino and Kasagi appear slightly higher than those of Kim and the present study, because their measurement was carried out at a relatively low Reynolds number.

The rms velocity fluctuations obtained independently in Figure 3 show a consistent change as the Reynolds number is increased. In this Reynolds number range, the peak value of u^+_{rms} exists in the buffer region and is almost constant, while those of v^+_{rms} and w^+_{rms} gradually move away from the wall and increase considerably in their values; these observations are also found in recent DNS results (Kim et al. 1987; Kim 1990, private communication; Kuroda et al. 1990; Kuroda et al. 1995).

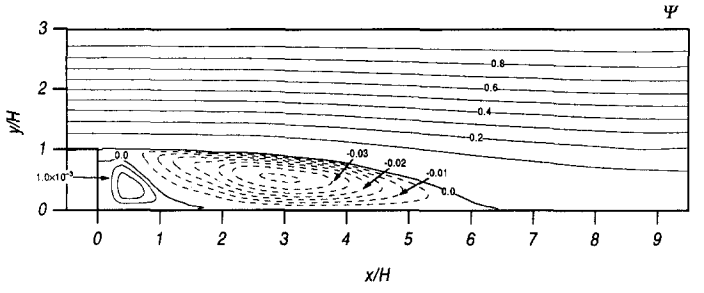

Figure 6 Streamlines

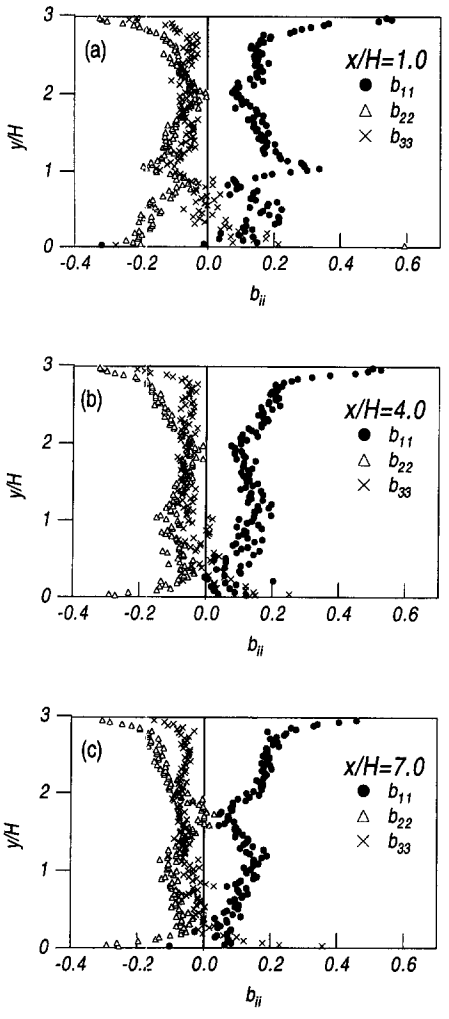

Figure 8 Normal components of stress anisotropy tensor: (a) $x/H = 1.0$, (b) $x/H = 4.0$, (c) $x/H = 7.0$

Reattachment length

It is evident that the point of separation is fixed at the step shoulder in the flow over a backward-facing step, but the point of reattachment may move back and forth as a function of time. Hence, the mean reattachment point is presently defined as the location where the time fraction of forward (streamwise) flow γ equals 0.5 toward the wall. In other words, the probabilities of positive and negative streamwise velocities should be exactly equal at the reattachment point. Although many velocity vectors have been obtained over the measurement region by the 3-D PTV, the number of vectors close to the wall is still insufficient for determining the forward flow fraction accurately. Hence, it has been calculated at various wall distances (with an interval of $0.01H$) in the region of $y/H = 0 \sim 0.4$ in the reattachment region. As a result, the point of $\gamma = 0.5$ at each streamwise location is obtained as shown in Figure 4, where the mean reattachment position is determined as $x_r = 6.51H$ by extrapolating the point of $\gamma = 0.5$ toward the wall. The present result is within the range of $6 \sim 8H$ estimated under the present experimental conditions by referring to Adams and Johnston's review (1988) of previous measurements.

Mean velocity distributions

The mean velocity distributions in the y direction at 11 streamwise locations are shown in Figures 5a and b. The streamwise mean velocity distribution at the step shoulder is almost the same as that of the fully developed channel flow measured upstream. Just downstream of the separation, where the separating shear layer is very thin, the velocity gradient in the y-direction is very steep, but it weakens gradually toward the reattachment point. In the recirculating region behind the step, the streamwise velocities are very small, but they have appreciable negative values in the near-wall region at $x/H = 2 \sim 5$; the maximum reverse flow velocity is about $0.2U_c$. It is noted that the flow rate, which is obtained as an integral of the streamwise velocity component over the cross section, is confirmed to be constant within $\pm 3\%$ over the whole streamwise distance and that there is no appreciable streamwise bulk flow acceleration (Kim et al. 1978) due to the developing boundary layer on the sides and corners of the duct. The mean velocity component normal to the wall V shows positive and negative peaks in the shear layer developing behind the step, but it becomes uniformly negative further downstream. This velocity component is a minimum at $x/H = 4 \sim 5$ and $y/H = 1$. In the recirculation zone, it has positive values from behind the step to about $x/H = 3$ and then changes to negative values downstream.

It is noted that greater data scatter around $x/H = 3$ is caused by the small sample size there; it is 30 to 70, which is an order of magnitude smaller than the average sample size. This particular position is located in a region of two overlapping measurement regions, but unfortunately the overlap was too small to produce sufficiently large sample size. Note also that although the mean spanwise velocities should be uniformly zero in 2-D flow, they show almost constant small values (~ 2.7 mm/s) because of the gravitational acceleration acting on the tracer particles. Therefore, every velocity vector obtained has been compensated for this nonzero spanwise velocity component.

The mean streamlines are shown in Figure 6; they are the contour lines of a stream function Ψ calculated by integrating the measured mean velocity components, which are very densely distributed in the present database. It is seen that the center of the main recirculating (eddying) region is located around $x/H = 3.0$ and $y/H = 0.6$. In addition, secondary separation takes place around $x/H = 1.7$. As a result, there appears a secondary recirculation region just downstream of the step, where the flow velocity is very small. Such a corner eddy has also been reported by previous investigators, e.g., Abbott and Kline (1962).

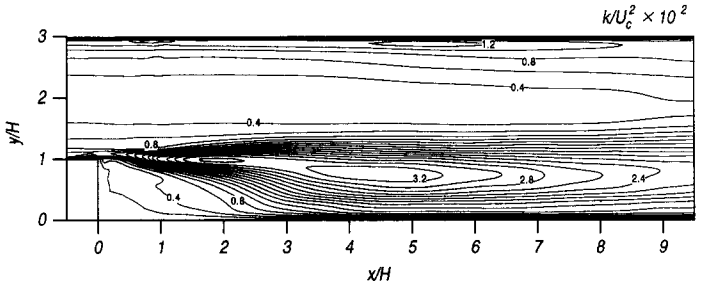

Figure 9 Contour lines of turbulent kinetic energy

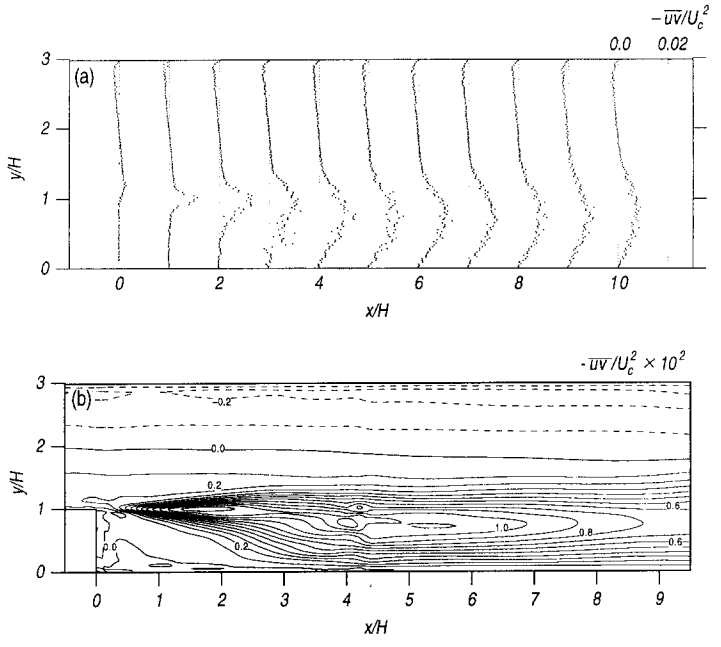

Figure 10 Reynolds shear stress: (a) cross-stream distributions, (b) contour lines

The dividing streamline shows a peculiar behavior during its final approach toward the reattachment point, i.e., its curvature changes abruptly near the wall around $x/H = 6.2$, and this makes the reattachment length slightly longer than the simply extrapolated value. This elongation of reattachment length is considered to be caused because the Reynolds shear stress; i.e., turbulent momentum transport, was considerably impeded by the presence of the wall, while the streamwise mean flow is accelerated in the reattachment region, as described below.

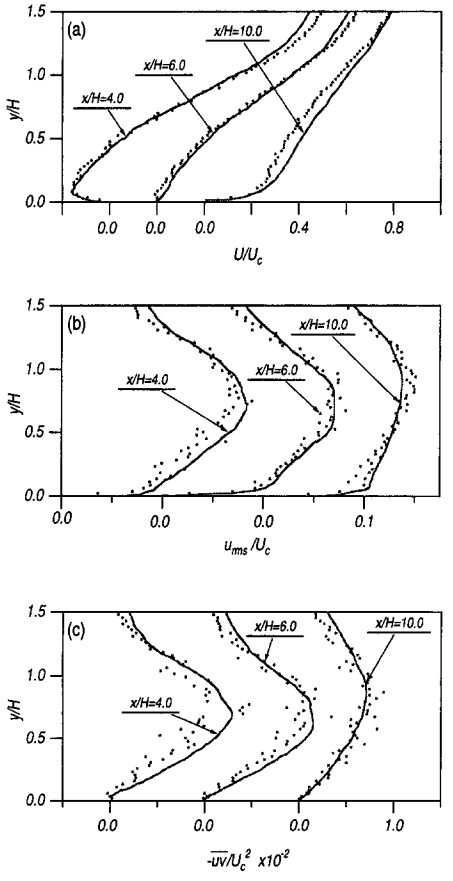

Figure 11 Comparison between present results and those of DNS by Le et al. (1993) (symbols, present experiment; lines, Le et al.): (a) mean velocity, (b) streamwise rms turbulent fluctuation, (c) Reynolds shear stress

Velocity fluctuations and turbulent kinetic energy

Root-mean-square velocity fluctuations are shown in Figure 7. The distribution of the streamwise component u_{rms} at the separation point in Figure 7a has two peaks near the walls and is similar to that of the upstream channel flow. While the distribution changes only moderately in the streamwise direction near the top wall, it exhibits a considerable change on the step side. The peak value first increases in the separated shear layer and, at $x/H = 1.5$ and $y/H = 1.0$, it reaches its maximum of almost 20% of U_c. While flowing downstream, the peak value position approaches closest to the wall, i.e., $y/H = 0.8$, at about $x/H = 4.5$, which is well upstream of the reattachment region. After that, it gradually shifts away from the wall and at the same time decreases in magnitude owing to diffusion of turbulent energy, and, eventually, a new peak arises near the wall.

In Figure 7b, the wall-normal component v_{rms} shows a distribution qualitatively similar to u_{rms} and also is maximum downstream of the separation point, but its magnitude is smaller than u_{rms}. The spanwise component w_{rms} is shown in Figure 7c. In almost all flow regions, as in the fully developed channel flow, w_{rms} is greater than v_{rms} but less than u_{rms}. In the recirculating region, however, w_{rms} becomes the greatest of the three components near the wall; this was first reported by Itoh and Kasagi (1989). Hence, the turbulent kinetic energy could not be estimated correctly from the two other components alone under an assumption such as $k = 3(u_{rms}^2 + v_{rms}^2)/4$, and independent measurement of w_{rms} is indispensable in separated and reattaching flows.

The above phenomena can be more clearly seen in the anisotropy tensor components, $b_{ij} = \overline{u_i u_j}/2k - \delta_{ij}/3$, of which typical distributions upstream and downstream of the reattachment point are shown in Figure 8. This is a measure of the turbulence anisotropy and is zero if a turbulence field is isotropic. In most of the flow field, b_{11} shows positive values, while b_{22} and b_{33} show negative values; i.e., the turbulent kinetic energy

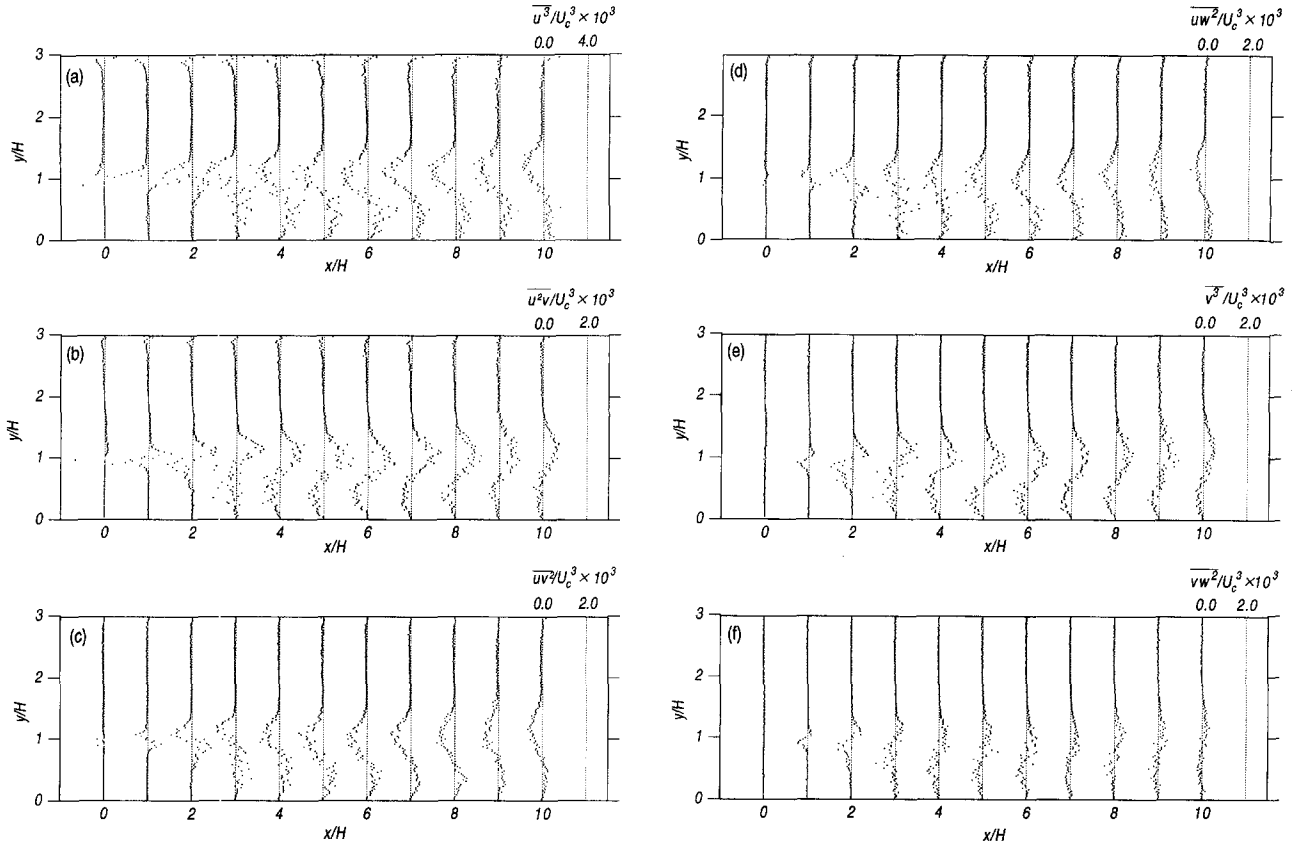

Figure 12 Triple velocity correlations: (a) $\overline{u^3}$, (b) $\overline{u^2v}$, (c) $\overline{uv^2}$, (d) $\overline{uw^2}$, (e) $\overline{v^3}$, (f) $\overline{vw^2}$

initially produced in the u component should be redistributed through the pressure–strain correlation to the v and w components. The results near the bottom wall, however, show a distinct distribution. Although it is natural that b_{22} decreases appreciably to large negative values owing to the wall-blocking effect, and consequently b_{11} and b_{33} have positive values, it is somewhat peculiar that b_{33} becomes larger than b_{11} without a direct production mechanism but only a redistribution mechanism for w. A plausible explanation is given as follows. From Figure 5, it is found that the wall-normal velocity gradient $\partial V/\partial y$ is negative, and hence $\partial U/\partial x$ is positive over a considerably wide region around the reattachment point. Thus, the vortex-stretching mechanism takes effect, so that the spanwise and wall-normal velocity fluctuations are intensified, while the streamwise component is attenuated. The wall-normal component, however, is damped by the presence of a wall and is also converted to the spanwise one. In addition, it is known that large-scale stream-wise vortices are formed in the reattachment (impinging) region of a turbulent shear layer (Kasagi et al. 1977; Neto et al. 1993; Yokobori et al. 1977). This provides an even more efficient mechanism of a strong pressure–strain correlation, by which the energy is redistributed to the spanwise component.

The contour lines of turbulent kinetic energy k are shown in Figure 9. As mentioned above, k is calculated exactly as a sum of all three components of turbulent intensity, and hence the distribution is more or less similar to those of turbulent intensities, especially that of the streamwise intensity. It is seen that k shows a sudden increase just downstream of the step, and the first maximum appears in the separating shear layer at $x/H = 2$. Further downstream at $x/H = 4.5$, there is another maximum. With the initial development of the shear layer, the turbulent kinetic energy diffuses toward the outer edges of the shear layer, where k gradually increases. The turbulent kinetic energy in the near-wall region becomes larger toward the reattachment point.

Reynolds shear stress

The distribution of the Reynolds shear stress, $-\overline{uv}$, is represented in Figures 10a and b. It is generally very similar to that of turbulent kinetic energy, particularly in the separating shear layer, but the shear stress changes its sign in the upper half of the channel. Near the upper wall at $y/H > 2$, the distribution is slightly different from that of the fully developed channel flow, and there seems to be little influence of the separation. In the recirculation region, the Reynolds shear stress is nearly equal to zero just behind the step, but downstream of $x/H = 3$, it increases appreciably. The other Reynolds shear stress components, $-\overline{vw}$ and $-\overline{uw}$, which should be zero in a 2-D flow, have been confirmed to be negligible in the present experiment. It is

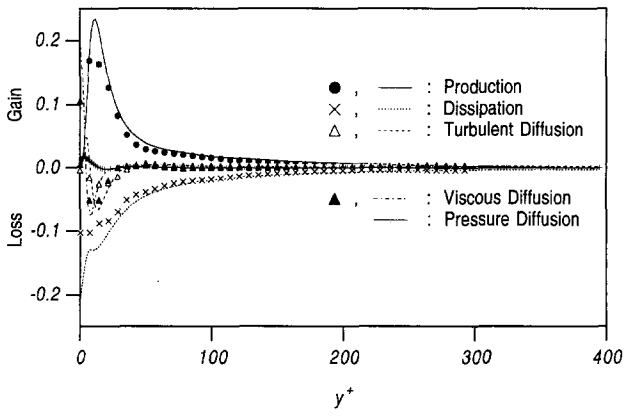

Figure 13 Budget terms for turbulent kinetic energy in fully developed channel flow, normalized by u_τ^4/ν (symbols, present experiment; lines, Kim 1990, private communication)

noted that the maximum values of u_{rms}/U_c and $-\overline{uv}/U_c^2$ are, respectively, 0.2 and 0.013, both of which are in good agreement with those reported by Eaton and Johnston (1981).

In Figure 11, the turbulent statistics presented above are compared with the DNS results of Le et al. (1993), who simulated a turbulent backward-facing step flow at a similar Reynolds number $U_bH/\nu = 5100$, but their inflow condition was a numerically simulated turbulent boundary layer flow of which the momentum thickness Reynolds number was 667. Thus, only a portion of the inflow was turbulent, unlike the present experiment. This resulted in their reattachment length of $6.0H$, which is slightly shorter than the present value of $6.51H$. With this in mind, it can be said that the present results and those of DNS of Le et al. should generally be in good agreement. The shorter reattachment length in the DNS gives slightly different profiles of the mean and fluctuating velocities, as well as of the Reynolds shear stress at $x/H = 10$, which suggest a faster transition to downstream channel flow.

Triple velocity correlations

All 10 components of triple velocity correlations were also calculated from the present database. Their spatial derivatives appear as turbulent diffusion terms in the transport equations of Reynolds stresses, and their accurate prediction is currently one of the major issues in second-order closure modeling. Four of them, $\overline{u^2w}$, $\overline{uvw}$, $\overline{v^2w}$, and $\overline{w^3}$, are zero in 2-D flow, and the measured values are also negligible. The distributions of the other six components are shown in Figure 12. Although some of them have opposite signs, they exhibit very similar distributions. That is, there are two peaks on both sides of the separating shear layer, and the peak on the upper side is larger than that on the lower side. It is obvious that, compared with channel flow (see, e.g., the top wall at $x/H = 0$), the triple velocity correlations are much greater in backward-facing step flow. Chandrsuda and Bradshaw (1981) reported that the triple velocity correlations decreased rapidly over the reattachment region, and hence the streamwise turbulent diffusion of Reynolds stresses should not be neglected. In contrast, the present results indicate that the change of the triple velocity correlations is moderate in the streamwise direction, and only the wall-normal turbulent diffusion should be appreciable.

Budget of turbulent kinetic energy

The transport equation of turbulent kinetic energy k is given as follows:

$$\frac{\partial k}{\partial t} = -U_j\frac{\partial k}{\partial x_j} - \overline{u_iu_j}\frac{\partial U_i}{\partial x_j} - \nu\frac{\overline{\partial u_i}}{\partial x_j}\frac{\overline{\partial u_i}}{\partial x_j} + \frac{\partial}{\partial x_j}\left(-\frac{1}{2}\overline{u_iu_iu_j} - \frac{1}{\rho}\overline{pu_j} + \nu\frac{\partial k}{\partial x_j}\right) \quad (1)$$

where the terms on the right-hand side are identified as convection, production, dissipation, turbulent diffusion, pressure diffusion, and viscous diffusion terms, respectively. Using the present database, all terms, except the viscous dissipation and pressure diffusion terms, can be calculated. If we neglect the pressure diffusion term, which is generally small compared with other terms,then the dissipation term can be estimated as the residual. When the spatial gradients in Equation 1 are calculated, spline fitting to the raw data is used.

The budget in the upstream channel flow is compared with the DNS result of Kim (1990, private communication) in Figure 13. The agreement between Kim's results and ours is fairly good, although there is some discernible difference in the vicinity of the wall where the number of velocity vectors measured is relatively small.

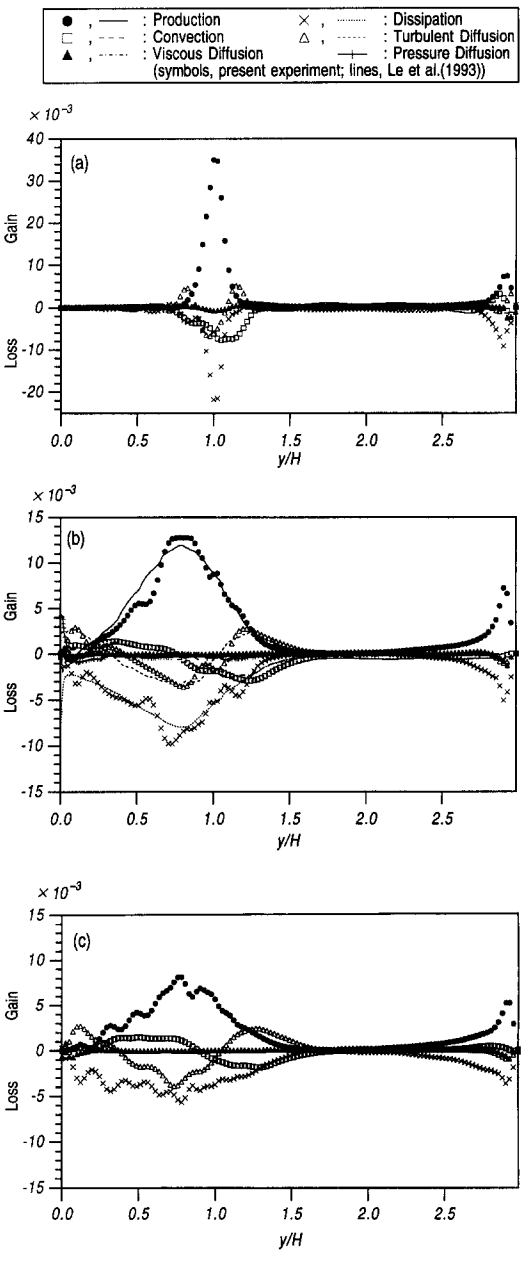

Figure 14 Budget terms of turbulent kinetic energy, normalized by U_c^3/H: (a) $x/H = 1$, (b) $x/H = 4$, (c) $x/H = 7$

The results downstream of the step are represented in Figure 14, where three typical cross-stream distributions are shown. In the separated shear layer at $x/H = 1$ in Figure 14a, the peak production rate becomes more than four times larger than that near the top wall. The convection and dissipation terms contribute negatively to the k budget, and the turbulent diffusion redistributes the energy from the central to the outer parts of the shear layer. Figures 14b and c, respectively, show the k budgets before and after the reattachment; i.e., at $x/H = 4$ and 7. With increasing streamwise distance, the maximum production rate decreases. In a 2-D flow, the production term in Equation 1 consists of the following four terms:

$$-\overline{u_iu_j}\frac{\partial U_i}{\partial x_j} = -\overline{u^2}\frac{\partial U}{\partial x} - \overline{uv}\frac{\partial U}{\partial y} - \overline{uv}\frac{\partial V}{\partial x} - \overline{v^2}\frac{\partial V}{\partial y} \quad (2)$$

Although not shown here, it was found separately that, over the entire region, the second term on the right-hand side of Equation 2 is the major contributor, while the third term can be neglected

totally. The first and fourth terms have almost the same magnitude but opposite signs, and hence the sum is relatively small (the sum is nonzero only when $\overline{u^2}$ is not equal to $\overline{v^2}$). For example, at $x/H = 6$ in the reattachment region, the magnitude of each of these two terms remains on the order of 10% of the second term at $y/H = 0.7 \sim 0.8$. However, because of a rapid decrease of $-\overline{uv}$ and $\partial U/\partial y$, the first term becomes the largest in the vicinity of the wall, $y/H < 0.15$. The turbulent diffusion term is still large, and it is a major contributor to the balance with the dissipation in the near-wall region, where the total production rate becomes smaller. This peculiar budget structure was also observed in the result of Pronchick and Kline (1983) and should be characteristic of separated and reattaching flow. It is noted that among the various turbulent diffusion terms, the y-derivatives are much larger than the x-derivatives.

In Figure 14b, the DNS result of Le et al. (1993) is also shown for comparison, and the agreement with the results from the present study is excellent. Thus, both PTV and DNS databases are accurate enough for testing and evaluating various turbulence models and numerical computations of this class of complex turbulent flows. Finally, it is surprising that the different inflow conditions of the present experiment and of the DNS of Le et al. resulted in little difference in the budget structure.

Conclusions

Using a 3-D particle-tracking velocimeter, detailed turbulence measurements were made in the separated and reattaching flow over a backward-facing step at the step Reynolds number of 5540. A fully developed turbulent channel flow was established well upstream of separation. As a result, a database of the turbulence statistics was established over a fairly wide region of $-2H$ upstream to $12H$ downstream of the step, including the recirculating and reattachment regions. The mean reattachment point defined based on the 50% forward flow fraction was $6.51H$. The calculated mean streamlines indicated a secondary corner bubble behind the step, where the flow is almost stagnant. The Reynolds normal and shear stresses had the maximum values in the separating free shear layer upstream of the reattachment. The Reynolds stress anisotropy tensor revealed a peculiar phenomenon near the reattachment wall, wherein even without a direct production mechanism, the spanwise normal stress was the largest among the three normal stress components. From the distributions of triple velocity correlations and the budget of turbulent kinetic energy, it was found that the turbulent diffusion plays a significant role in the transport of Reynolds stresses, especially in the separating shear layer and in the reattachment region. The present results of mean and fluctuating velocities, the Reynolds shear stress, and the turbulent energy budget were compared with those of the DNS of Le et al. (1993); the agreement was excellent. This was somewhat surprising, because there was a considerable difference in the inflow conditions.

Acknowledgments

The authors are grateful to Sin-ichi Kawara at Tokyo Gas Co., Ltd. for his cooperation during the course of this work.

References

Abbott, D. E. and Kline, S. J. 1962. Experimental investigation of subsonic turbulent flow over single and double backward facing steps. Trans. ASME, *J. Basic Eng.*, **84**, 317–325

Adams, E. W. and Johnston J. P. 1988. Effects of the separating shear layer on the reattachment flow structure. *Exp. Fluids*, **6**, 493–499

Akselvoll, K. and Moin, P. 1993. Large eddy simulation of a backward facing step flow. In *Engineering Turbulence Modelling and Experiments 2*, W. Rodi and F. Martelli (eds.). Elsevier, New York, 303–313

ANSI/ASME PTC 19.1-1985. Part 1, Measurement Uncertainty: Instruments and Apparatus, New York: The American Society of Mechanical Engineers, 1986

Chandrsuda, C. and Bradshaw, P. 1981. Turbulence structure of a reattaching mixing layer. *J. Fluid Mech.*, **110**, 171–194

Dean, R. B. 1978. Reynolds number dependence of skin friction and other bulk flow variables in two-dimensional rectangular duct flow. *J. Fluids Eng.*, **100**, 215–223

Driver, D. M. and Seegmiller, H. L. 1985. Features of a reattaching turbulent shear layer in divergent channel flow. *AIAA J.*, **23**, 163–171

Eaton, J. K. and Johnston, J. P. 1981. A review of research on subsonic turbulent flow reattachment. *AIAA J.*, **19**, 1093–1100

Itoh, N. and Kasagi, N. 1989. Turbulence measurement in a separated and reattaching flow over a backward-facing step with the three-dimensional particle tracking velocimeter (in Japanese). *Nagare-no Kashika* (J. Flow Visualization Soc. Jpn.), **34**, 245–248

Kasagi, N., Hirata, M. and Hiraoka, H. 1977. Large-eddy structures in turbulent separated flow downstream of a rearward-facing step. *Proc. Symposium Turbulent Shear Flows*, The Pennsylvania State University, University Park, PA, 16.14

Kasagi, N. and Nishino, N. 1991. Probing turbulence with three-dimensional particle-tracking velocimetry. *Exp. Therm. Fluid Sci.*, **4**, 601–612

Kasagi, N. and Sata, Y. 1992. Recent developments in three-dimensional particle tracking velocimetry. *Proc. 6th international symposium on flow visualization*, Yokohama, 832–837

Kawara, S. and Kasagi, N. 1989. Turbulence measurement in the separated and reattaching flow downstream of a step with the aid of 3-D particle tracking velocimeter (in Japanese). *JSME* Preprint, No. 895-50, 293–294

Kim, J., Kline, S. J. and Johnston, J. P. 1978. Investigation of separation and reattachment of a turbulent shear layer: Flow over a backward-facing step. Rpt. MD-37, Mech. Eng. Dept., Stanford University, Stanford, CA

Kim, J., Moin, P. and Moser, R. 1987. Turbulent statistics in fully developed channel flow at low Reynolds number. *J. Fluid Mech.*, **177**, 133–166

Kuroda, A., Kasagi, N. and Hirata, M. 1990. A direct numerical simulation of the fully developed turbulent channel flow. In *Numerical Methods in Fluid Dynamics*, M. Yasuhara et al. (eds.), *J. Soc. Comp. Fluid Dyn.*, 1012–1017

Kuroda, A., Kasagi, N. and Hirata, M. 1995. Direct numerical simulation of turbulent plane Couette–Poiseuille flows: Effect of mean shear rate on the near-wall turbulence structures. In *Turbulent Shear Flows 9*, F. Durst et al. (eds.) Springer-Verlag, Berlin, 241–257

Le, H., Moin, P. and Kim, J. 1993. Direct numerical simulation of turbulent flow over a backward-facing step. *Proc. 9th symposium on turbulent shear flows*, Kyoto, Japan, 13.2.1–13.2.6

McEligot, D. M. 1984. Measurement of wall shear stress in accelerating turbulent flows, Max-Planck Institut für Strömungsforschung, Göttingen, Germany

Neto, A. S., Grand, D., Metais, O. and Lesieur, M. 1993. A numerical investigation of the coherent vortices in turbulence behind a backward-facing step. *J. Fluid Mech.*, **256**, 1–25

Ninomiya, N. and Kasagi, N. 1993. Measurement of the Reynolds stress budgets in an axisymmetric free jet with the aid of three-dimensional particle tracking velocimetry. *Proc. 9th symposium on turbulent shear flows*, Kyoto, Japan, 6.1.1–6.1.6

Nishino, N. and Kasagi, N. 1989. Turbulence statistics measurement in a two-dimensional channel flow using a three-dimensional particle tracking velocimeter. *Proc. 7th symposium on turbulent shear flows*, Stanford, CA, 22.1.1–22.1.6

Nishino, K., Kasagi, N. and Hirata, M. 1989. Three-dimensional particle tracking velocimetry based on automated digital image processing. *J. Fluids Eng.*, **111**, 384–391

Pronchick, S. W. and Kline, S. J. 1983. An experimental investigation of the structure of a turbulent reattaching flow behind a backward-facing step. Rep. MD-42, Mech. Eng. Dept., Stanford University, Stanford, California

Yokobori, S., Kasagi, N. and Hirata, M. 1977. Characteristic behavior of turbulence in the stagnation region of a two-dimensional submerged jet impinging normally on a flat plate. *Proc. symposium on turbulent shear flows*, The Pennsylvania State University, University Park, PA, 3.17–3.25